◆ Human Brain Mapping 35:2582–2593 (2014) ◆

Altered Resting-State Connectivity in Huntington's Disease

Cornelius J. Werner,[1,3†] Imis Dogan,[1,2,3†] Christian Saß,[1,4] Shahram Mirzazade,[1,2,3] Johannes Schiefer,[1] N. Jon Shah,[1,2,3] Jörg B. Schulz,[1,3] and Kathrin Reetz[1,2,3*]

[1]*Department of Neurology, RWTH Aachen University, Aachen, Germany*
[2]*Institute of Neuroscience and Medicine, Research Center Jülich, Jülich, Germany*
[3]*JARA BRAIN – Translational Brain Medicine, Jülich and Aachen, Germany*
[4]*Department of Neurology, Asklepios Hospital Hamburg, Hamburg, Germany*

Abstract: Huntington's disease (HD) is an autosomal dominantly inherited neurodegenerative disorder characterized by motor, cognitive, and psychiatric symptoms. Using resting-state fMRI (rs-fMRI) we investigated the functional integrity of resting-state networks (RSN) in HD. 17 HD and 19 matched control participants were examined at a 3 Tesla MR scanner. After controlling for structural degeneration by means of voxel-based morphometry, task-free rs-fMRI data were analyzed using Independent Component Analysis (ICA) and a dual-regression approach in the context of genetic and clinical parameters. Further, we evaluated HD-related differences in interregional connectivity between networks. RSN analysis showed a significant increase in intrinsic functional connectivity in the HD sample compared with controls, including the thalamus, striatum, prefrontal, premotor, and parietal maps. A subset of the Default Mode Network (DMN) was also affected. In the HD cohort, motor impairment correlated with higher network connectivity in mainly motor and parietal cortices. Deteriorating total functional capacity was additionally associated with higher connectivity in the striatum, thalamus, insular and frontal areas. This pattern of increased activity in intrinsic functional networks might suggest a reduced ability of intra-network differentiation with clinical disease progression in HD. Finally, results showed reduced long-range connectivity between parietal ICA components in HD compared to controls, indicating impaired functional coupling between interregional networks in HD. Our data demonstrates that functional connectivity is profoundly altered in HD, both within and between RSN. Rs-fMRI analysis may provide additional valuable insights into neuronal dysfunctions beyond HD-related structural degeneration and disruptions of functional circuits in HD. *Hum Brain Mapp 35:2582–2593, 2014.* © 2013 Wiley Periodicals, Inc.

Additional Supporting Information may be found in the online version of this article.

Contract grant sponsor: Excellence Initiative of the German federal and state governments; Contract grant number: DFG ZUK32/1; Contract grant sponsor: IZKF Aachen (Interdisciplinary Center for Clinical Research within the Faculty of Medicine at the RWTH Aachen University)

*Correspondence to: Kathrin Reetz, Department of Neurology, RWTH Aachen University, Pauwelsstrasse 30, D-52074 Aachen, Germany. E-mail: kreetz@ukaachen.de

†The authors contributed equally to this work.

The study was approved by the Ethics committee of the Medicine Faculty of the RWTH Aachen University, and conducted in agreement with the Declaration of Helsinki. All participants gave written informed consent.

Received for publication 2 March 2013; Revised 8 May 2013; Accepted 29 May 2013.

DOI: 10.1002/hbm.22351

Published online 24 August 2013 in Wiley Online Library (wileyonlinelibrary.com).

Key words: resting-state fMRI; default mode network; functional connectivity; structural degeneration; voxel-based morphometry; Huntington's disease; neurodegenerative diseases

INTRODUCTION

Huntington's disease (HD) is an autosomal dominantly inherited, progressive neurodegenerative disorder caused by an expanded trinucleotide CAG sequence in exon 1 of the huntingtin gene (HTT). Although huntingtin is expressed ubiquitously, the expression of huntingtin with a polyglutamine repeat expansion leads to selective neuronal cell death in the striatum and cortex. Clinically, HD is characterized by the development of progressive motor dysfunction, cognitive decline, and psychiatric disturbances. To date, there is no neuroprotective treatment to slow down disease progression, highlighting the need for novel insights into early cell dysfunctions in this devastating disease.

Magnetic resonance imaging (MRI) techniques are appealing as noninvasive biomarkers as they allow an objective assessment of alterations in the diseased brain that may provide potential targets in disease-modifying treatment trials. These techniques have shown sensitivity to detect altered structure or physiology within the brains of individuals with premanifest and early HD, sometimes many years before clinical disease onset. Task-based functional MRI (fMRI) studies have revealed aberrant functional networks before overt cell death and in the absence behavioral deficits, indicating that neural dysfunctions precede structural degeneration and may hence hold important clues to the pathophysiology of HD. Resting-state fMRI (rs-fMRI) has a strong clinical appeal because it is easily applicable and allows to study multiple brain networks at rest without confounding effects of cognitive ability to perform a given behavioral task [Fox and Raichle, 2007; Greicius, 2008]. Rs-fMRI measures spontaneous fluctuations in the BOLD signal, which enables us to investigate the functional connectivity between brain regions showing a temporal coherence in these fluctuations, giving rise to so-called resting-state networks (RSNs). Although there has been an enormous increase in rs-fMRI in clinical populations, especially in neurodegenerative disorders [Fox and Greicius, 2010], data on task-free rs-fMRI using Independent Component Analysis (ICA) to investigate functional brain integrity including the "Default Mode Network" (DMN) in HD are still lacking. One particular challenge might be the marked cerebral atrophy in these patients [Dogan et al., 2012; Tabrizi et al., 2009; Tabrizi et al., 2011; Tabrizi et al., 2012] and the clinical heterogeneity in spite of the monogenetic etiology, potentially confounding functional imaging results. Hence, we here performed a combined structural and rs-fMRI study to evaluate HD-related intrinsic functional connectivity networks and critical network hubs (RSNs) while controlling for structural gray matter volume loss and further investigated the relation to markers of disease progression (i.e., motor, genetic and functional parameters).

MATERIALS AND METHODS

Participants

Seventeen HD patients with a genetically confirmed abnormal number of CAG repeats (40–49) were recruited from our Huntington Outpatient Clinic (Department of Neurology, RWTH Aachen University, Germany). The control group comprised 19 healthy volunteers with no history of neurological or psychiatric diseases and did not differ significantly from the HD group with respect to age, gender, handedness or educational level (see Table I for a detailed description of sample characteristics). All subjects gave their written informed consent for participation in this study, which was approved by the local ethics committee according to the declaration of Helsinki.

Participants were examined using the Unified Huntington's Disease Rating Scale [UHDRS, Huntington Study

TABLE I. Demographics, clinical, and neuropsychological scores for HD patients and controls

	HD group (n = 17)		Controls (n = 19)		
	Mean	SD	Mean	SD	P-value
Age (in years)	44.9	9.9	47.5	10.1	0.448
Gender (male/female)	7/10		8/11		0.955[a]
Handedness (R/L)[b]	15/2		17/2		0.906[a]
Education (ISCED)	3.0	0.6	3.5	0.8	0.093[d]
CAG repeat length	44.2	2.6	n.a.	n.a.	
Disease Burden[c]	376.7	79.2	n.a.	n.a.	
MMSE	27.6	1.9	29.1	0.7	0.002[d]
UHDRS: Motor	31.1	20.2	1.0	1.0	<0.001
TFC	10.1	2.7	13.0	0	<0.001[d]
Behavior	15.5	11.9	2.3	3.1	<0.001
Cognitive total score	208.7	81.1	319.3	35.9	<0.001
Verbal fluency	28.6	16.1	40.4	9.3	0.014
Symbol digit	33.4	15.1	52.6	11.8	<0.001
Stroop	146.7	54.0	226.3	23.7	<0.001

SD, standard deviation; ISCED, International Standard Classification of Education (1997); MMSE, Mini Mental State Examination; UHDRS, Unified Huntington's Disease Rating Scale; TFC, Total functional capacity score; n.a., not applicable

[a]Chi-square test.

[b]based on the Edinburgh Inventory (Oldfield, 1971)

[c]Age x (CAG – 35.5) based on Penney et al. (1997).

[d]Mann-Whitney U-test (remaining group comparisons assessed with 2-sample T-tests).

Group, 1996] for each subscale (motor, function, total functional capacity (TFC), behavior, cognition) and the Mini-Mental-State Exam [MMSE, Folstein et al., 1975]. Three HD mutation carriers were presymptomatic (UHDRS-motor score < 5), most of the remaining patients were in an early disease stage (stage I/II; TFC ≥ 7), while three patients were in a moderate stage III [Shoulson and Fahn, 1979]. Four patients showed depressive mood symptoms in the UHDRS-behavior assessment, but none were suffering a severe depressive episode at the time of study participation. All participants were autonomous (UHDRS-independence scale $\geq$75%) and showed no signs of dementia. UHDRS-cognitive assessment revealed impairments in the HD group compared to controls in all subscales (Phonetic Verbal Fluency, Symbol Digit Modalities, Stroop Interference tests). To assess the burden of disease pathology and its influence on neural activity, we used the index of disease-burden based on the formula *Age*[CAG–35.5]* [Penney et al., 1997]. This score provides a measure of genetic disease load while taking account of subjects' current age, and was shown to strongly correlate with HD-related clinical features [Tabrizi et al., 2009].

MRI Data Acquisition

For functional data acquisition, subjects were scanned in a 3-Tesla Trio MRI scanner (Siemens Medical Systems, Erlangen, Germany) for ~10 min yielding 270 volumes of measurement with the following parameters: EPI gradient echo images, TR 2,200 ms, TE 30 ms, slice thickness 3.1mm, matrix 64 x 64, FoV = 200 mm. Additional high-resolution T1-weighted MP-RAGE images were acquired for each subject using the following parameters: TR = 1,900 ms, TE = 2.5 ms, matrix size = 256 x 246, 176 sagittal slices, voxel size = 1 x 1 x 1 mm^3, field of view = 250 x 250 mm^2. In order to avoid visual stimulation during scanning, subjects were wearing MR-compatible goggles displaying a black screen, and were instructed to move as little as possible and not to fall asleep. Post-scan debriefing confirmed compliance with the instructions.

Analysis of Structural Imaging Data

To investigate structural differences between HD patients and controls, T1-weighted images were analyzed with FSL, a VBM style analysis [Ashburner and Friston, 2000; Smith and Nichols, 2009] carried out with FSL tools (http://www.fmrib.ox.ac.uk/fsl/fslwiki/FSLVBM) in an almost fully automated fashion. Briefly, structural images were first segmented into gray matter, white matter and cerebrospinal fluid. The resulting gray-matter partial volume images were then aligned to MNI152 standard space using an affine registration tool and averaged to create a study-specific template, to which the native gray matter images were then non-linearly re-registered. The registered partial volume images were then modulated (to correct for local expansion or contraction) by dividing by the Jacobian of the warp field and smoothed with an isotropic Gaussian kernel with a sigma of 6 mm. Finally, gray matter differences between patients and controls were assessed using permutation-based non-parametric testing incorporating threshold-free cluster enhancement (TFCE) [Smith and Nichols, 2009]. Age was entered as nuisance regressor and resulting statistical maps were thresholded at $p \leq 0.001$ (TFCE-corrected for family wise errors).

From the structural data, we also derived voxel-wise gray matter nuisance regressors for each subject, which were used in all functional data analyses to account for structural differences on the individuals' voxel level, following the method proposed by Oakes et al. [2007]. Briefly, after tissue-type segmentation using FAST implemented in FSL 4.1, gray matter images were normalized into standard space and demeaned across the whole group, after which they were entered as regressors of no interest in subsequent analyses of rs-fmri data.

Analysis of Short-Range Resting State Functional Connectivity

Group differences in RSN integrity were analyzed using MELODIC (Multivariate Exploratory Linear Decomposition into Independent Components, Version 3.09), and a subsequent dual regression analysis as described previously [Filippini et al., 2009; Smith et al., 2009; Zuo et al., 2010]. In detail, the following steps were applied: Standard prestatistical processing was performed including brain extraction, motion correction, spatial smoothing (FWHM 6 mm) and high-pass temporal filtering (sigma 100 s), using the respective tools in FSL (FMRIB's Software Library, www.fmrib.ox.ac.uk/fsl). Functional data were linearly coregistered into standard MNI space via the individuals' structural scans. Preprocessed data were concatenated temporally and then decomposed into spatially independent maps representative for the whole study sample using probabilistic Principal Component Analysis with automatic estimation of number of dimensions and variance normalization enabled [Beckmann and Smith, 2004; Smith and Nichols, 2009]. Estimated component maps were thresholded with a probability of $p > 0.5$ by fitting a mixture model to the histogram of intensity values. Voxels with a mixture-modelling Z-score > 4 belonging to the respective maps were plotted on a standard MNI-152 brain. Components of interest were identified by visually inspecting their temporal characteristics and by assessing neuroanatomical plausibility (e.g., striatum). Additionally, we visually compared them to a set of 70 previously published "canonical" resting state components [Smith et al., 2009], (retrieved from http://fsl.fmrib. ox.ac.uk/analysis/brainmap+rsns).

Dual regression analysis was then performed as follows: all ICA maps (including artifactual ones) were spatially regressed against the individual fMRI data sets to identify matrices describing subject- and map-specific time-courses. These time-courses were used to estimate the respective

spatial map for each subject (temporal regression) in terms of voxel-wise z-scores. On the basis of the previous work by Smith et al. [2009], we selected those maps that most closely resembled known and neuroanatomically meaningful RSNs for further analysis employing nonparametric randomization techniques. The first analysis aimed at testing for significant differences across groups, while the second analysis tested for correlations between clinical measures (UHDRS motor and cognitive scores, TFC and CAG repeat length) and RSN connectivity measures as represented by the respective z-scores.

All analyses were carried out using nonparametric permutation testing with 10.000 permutations [Nichols and Holmes, 2002; Smith and Nichols, 2009; Zhang and Raichle, 2010]. Subjects' age as well as voxel-wise gray matter values (correcting for atrophy) were entered as regressors of no interest in all analyses. All analyses of RSN integrity were restricted to the spatial extent of the group-representative RSN map in question itself derived from the whole sample (thresholded at $z > 4$), thus effecting a "region of interest"-analysis. By limiting ourselves to values within the RSNs in such a manner, results of this analysis could then be regarded as a measure of RSN-intrinsic integrity.

As we tested a multitude of RSNs in several tests, we addressed the issue of multiple testing by controlling the false discovery rate (FDR) at $p \leq 0.05$ [Benjamini and Yekutieli, 2001].

Analysis of Long-Range Functional Connectivity

Apart from testing differences in regional (short-range) RSN integrity between groups, we were also interested in the temporal relation between resting state networks, potentially indicating integrity (or lack thereof) of long-range connections in HD. To obtain further connectivity information between RSN, we applied the "FSLNets" package (http://fsl.fmrib.ox.ac.uk/fsl/fslwiki/FSLNets) implemented in Matlab (http://www.mathworks.de). This package accomplished the following steps: First, the respective time courses of all maps in each of the subjects were extracted and then normalized by subjects' standard deviations. Time courses of artifactual components and components of no interest (such as physiological noise) were regressed out of the individual data. We then created subject-wise correlation matrices of both full correlation and partial correlation of all remaining RSN time courses. Resulting Fisher's r correlation coefficients were z-transformed and corrected for temporal autocorrelation. This yielded individual correlation matrices of all components, representing neuronal signal corrected for the influences of artefactual components. P-scores expressed the functional connectivity values between entire RSNs (acting as the nodes in this network) on a long-range scale, traversing entire lobes or hemispheres. After averaging all individual correlation matrices, we clustered the resulting nodes hierarchically by using the information about temporal similarity of the full correlation matrices. Results are plotted in a dendrogram (Fig. 4).

These data were used to test for differences in connection strengths across groups. To achieve this, we subjected the individual partial correlation values (which can be seen to represent "direct" connections better than the full correlation values) to a General Linear Model, using age as a confound regressor. Only those connections were tested that were strong on average in all subjects by pre-masking the partial-correlation matrix using a t-value > 8. Results were corrected for multiple testing by applying a family-wise error (FWE) correction, thresholded at $p \leq 0.05$.

Analysis of Motion Artifacts

Recently, there has been considerable interest in assessing the effect of motion on rs-fMRI results. In particular, it has been shown for seed-based resting-state analyses that motion affects connectivity values even after performing standard and advanced correction methods such as spatial realignment and regression of motion estimates [Power et al., 2012]. Power et al. [2012] cautioned that noise introduced by residual motion might lead to an overestimation of short-range connectivity and under-estimation of long-range connectivity. To assess the effect of motion in our ICA approach, we extracted the subject-wise absolute displacement values in mm, which describe the absolute amount of movement in all directions (akin to a sum vector) over the whole scan as a marker of gross motion. Additionally, volume-wise relative displacement values (in mm) were extracted, which measures the amount of movement between one EPI volume and the next as a marker of micro-motion. Both variables were averaged across volumes (relative displacement) and subjects (relative and absolute displacement) and then subjected to a two-sample t-test in order to assess differences in motion across groups. Additionally, we correlated subject-wise absolute and relative displacement values with UHDRS motor scores using Spearman's rank correlation coefficient to investigate the association between subject motion and clinical motor impairment, including chorea.

In a second step, we correlated relative displacement values with all ICA timecourses in a given subject and then averaged correlation values across subjects, yielding one average correlation coefficient per ICA. This was done to assess the impact of motion on ICA timecourses as these were the basis of all further analyses. Absolute and relative displacement values were created by MCFLIRT software as part of FSL. All analyses were performed using R statistical software (www.r-cran.org).

RESULTS

Structural Differences Between HD Patients and Controls

VBM analysis of volume reductions in HD patients compared with controls revealed gray matter atrophy in patients in the bilateral striatum, insula, parietal

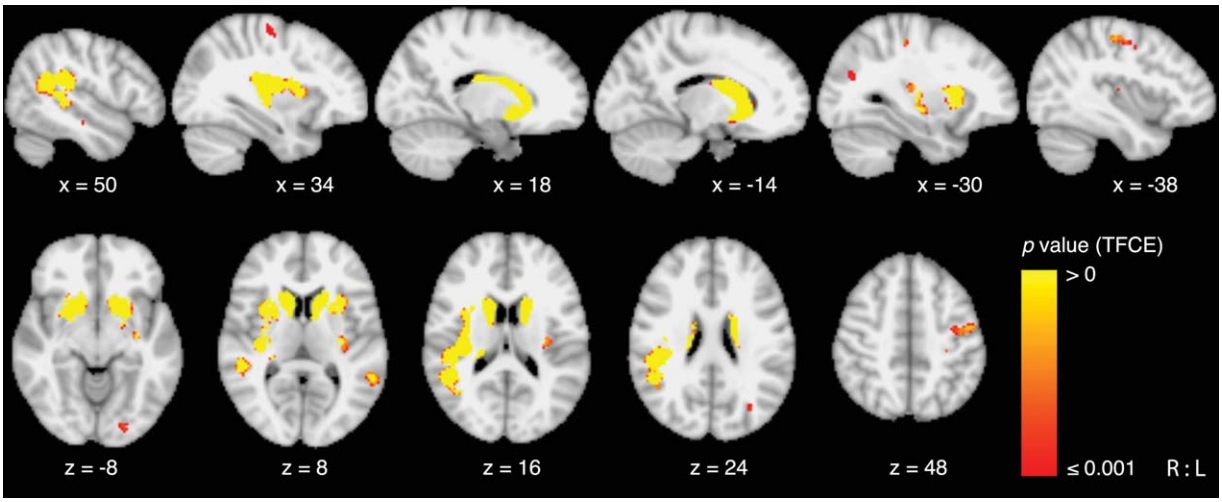

Figure 1.
Significant gray matter volume reductions in HD patients compared to controls as revealed by VBM. R/L: right/left. Coordinates in MNI space.

operculum, middle temporal gyrus, left inferior parietal cortex, premotor cortex and sensorimotor cortex (TFCE-corrected $p \leq 0.001$; Fig. 1, for detailed description of cluster maxima and anatomical regions see Supporting Information Table S-I).

Short-Range Resting-State Networks: Between-Group Differences

Eighty-two components were identified in the full sample, of which 24 were deemed to represent neuronal signal. Among these RSN, 11 showed a significant increase in intrinsic functional connectivity in the HD sample compared to controls (FDR-corrected $p < 0.05$; Fig. 2, Supporting Information Table S-II). These included three subcortical ICA maps located in the bilateral thalamus (mainly prefrontal, parietal and temporal connectivity zones [Behrens et al., 2003], the bilateral caudate and putamen extending to the pallidum and amygdala. Additionally, we found one RSN located in the posterior and one in the anterior cerebellum. Cortically, patients exhibited an increase in resting-state connectivity in the medial and lateral prefrontal cortex, cingulate cortex, supplementary motor area, and premotor cortex. In parietal regions we identified three ICA maps showing significant increases in HD patients compared with controls, including the superior parietal lobule bilaterally, intraparietal sulcus, inferior parietal cortex, angular gyrus, precuneus, and left somatosensory cortex (Brodmann area (BA) 2). These maps also extended to middle temporal and superior/middle occipital gyri (Fig. 2, Supporting Information Table S-II). Notably, the DMN seems to be split up into two parts in our analyis, namely components 38 and 43, together encompassing the core regions of the DMN such as precuneus, lateral parietal cortex and anterior cingulate cortex (IC 43), and more distant, but well-described regions such as parieto-occipital cortex together with fusiform/parahippocampal gyrus (IC 38; see also below for further corroboration) [Raichle et al., 2001; Raichle and Snyder, 2007]. Of these, in particular parietooccipital regions of IC 38 within the DMN were affected by HD-related alterations.

There were no ICA maps in which patients exhibited reduced functional connectivity compared to controls. Note that we reanalyzed resting-state connectivity for the symptomatic sample only after excluding the three presymptomatic HD mutation carriers (and adjusting the control cohort accordingly with respect to sociodemographic features). Here, almost identical ICA maps were obtained in this analysis with significant increases in functional connectivity in corresponding regions in the HD group compared to controls (Supporting Information Table S-II).

Short-Range Resting-State Networks: Correlations with Clinical and Genetical Parameters

In a natural extension of the analysis above, we were interested whether an increase or decrease in functional connectivity might convey clinical benefits in terms of TFC or motor and cognitive abilities as measured by the UHDRS. In a similar vein, it might be argued that the CAG repeat length has a linear (or at least monotonous) impact on functional connectivity values. Thus, correlations of functional connectivity values with clinical scores were tested. We found that within the HD sample, there was a total of 61 components, 19 of which were compatible with neuronal resting state networks, mostly identical to the maps of the full-sample analysis.

Higher UHDRS-motor scores were correlated with an increase of network connectivity in five RSNs, including

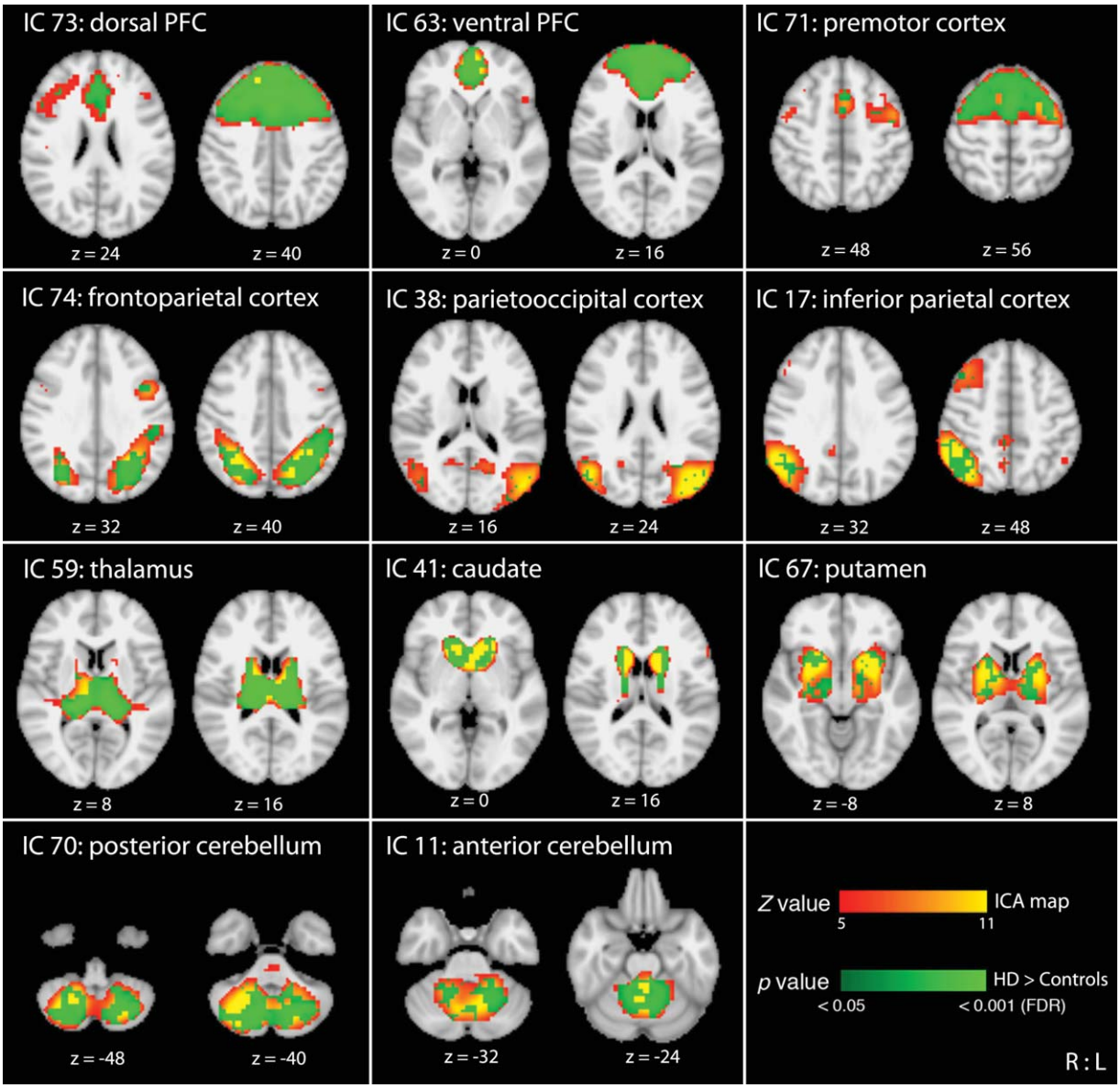

Figure 2.

Resting-state networks showing a significant increase in intrinsic functional connectivity in the HD sample compared to controls. Red/yellow: independent components (IC) identified in the full sample; in green: significant between-group differences. PFC, prefrontal cortex; R/L: right/left. Coordinates in MNI space.

the supplementary motor area, premotor and sensorimotor cortex, the superior and inferior parietal cortex, intraparietal sulcus, precuneus and cuneus, superior occipital gyrus, middle cingulate cortex and right insula (Fig. 3A, Supporting Information Table S-III). In terms of abilities of every-day life, lower TFC scores were correlated with higher connectivity values in 11 components, mostly identical to the RSNs seen in the correlation with UHDRS-motor scores and additionally including the bilateral insula and left frontoparietal regions (including Broca's area, parietal operculum). Connectivity in the calcarine gyrus (BA17, 18), bilateral thalamus and striatum was also associated with worse TFC scores (Fig. 3B, Supporting Information Table S-III). The component that most closely resembled the core set of regions making up the DMN in the previously published dataset [Smith et al., 2009] marginally failed to reach significance (FDR $p = 0.056$) in this correlational analysis. Surprisingly, we did not find any

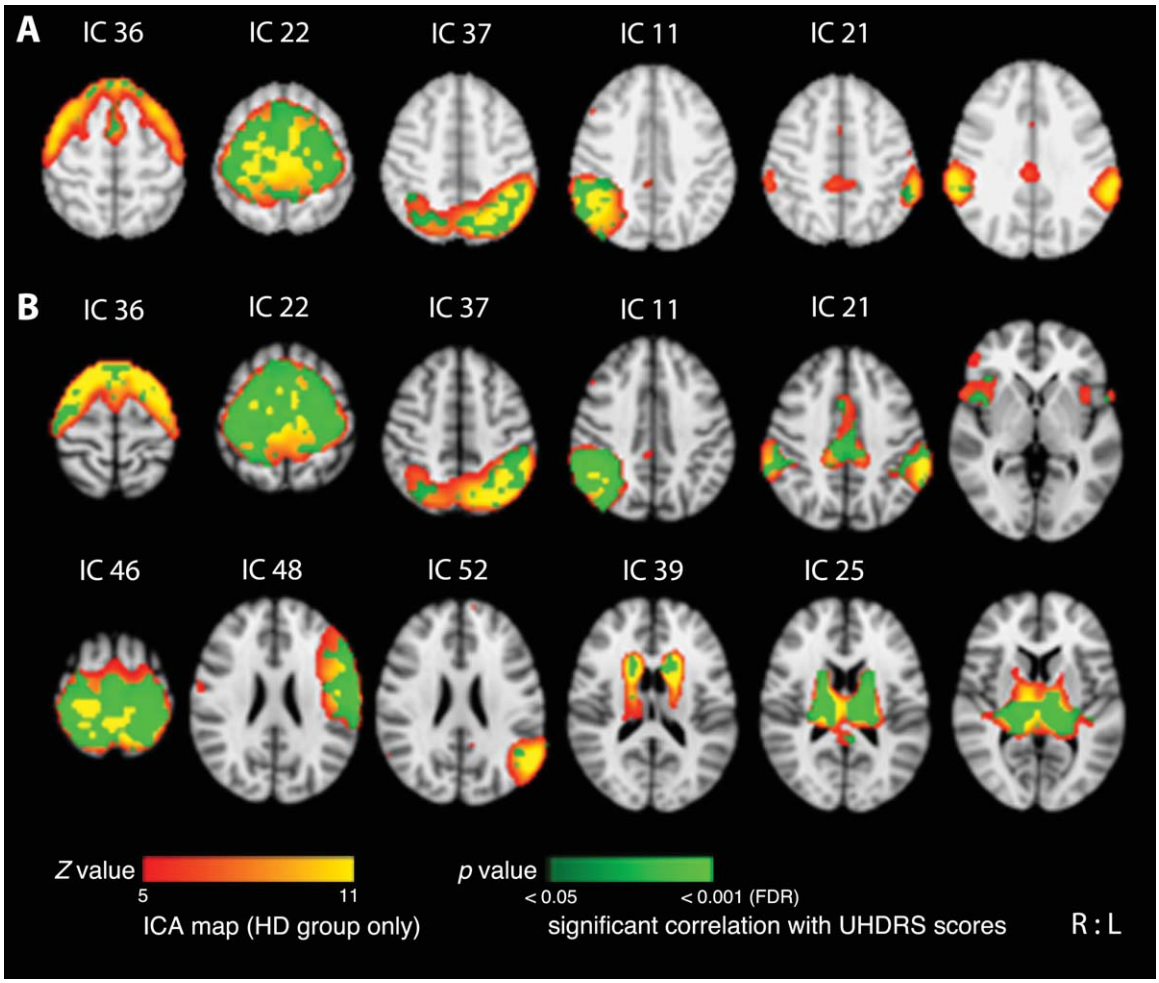

Figure 3.

Significant correlations between higher resting-state connectivity and clinical scores. Red/yellow: independent components (IC) identified in the HD sample; in green: **A** positive correlation with UHDRS-motor scores, **B** negative correlation with UHDRS-total functional capacity. R/L: right/left.

significant correlations (or anti-correlations) with cognitive scores, CAG repeat length or disease burden scores.

Long-Range Functional Connectivity

In our sample, the RSNs could be grouped into three main clusters (Fig. 4) according to their connectivity patterns with each other. One cluster (green lines) contained the DMN along with fronto-parietal RSNs. The DMN itself seemed to consist of two components in our sample, with the core features such as precuneus and lateral parietal cortices ending up in component 43, and the part comprising parietooccipital cortex and parahippocampal/ fusiform gyrus being spatially segregated into component 38. The time-courses of those two components were highly correlated, however, indicating tight functional coupling. In our analysis, component 38 was hit specifically by HD pathology, indicating that subsets of the DMN can be affected independently from each other.

The second cluster mainly comprised primary and secondary/higher order visual cortices (blue lines), whereas the third cluster of RSNs contained motor, premotor, frontal, thalamic, striatal/caudate as well as cerebellar RSNs (red lines), thus basically making up the fronto-striato-thalamo-cerebellar circuitry of the brain. It was this cluster where the most significant alterations were taking place within the respective RSNs as shown in the short-range analysis above, with thalamus, prefrontal cortex and striatum showing the most significant changes across groups (see Supporting Information Table S-2).

With respect to functional connectivity values between RSNs as a marker of long-range functional connectivity, we found significant differences in the connection

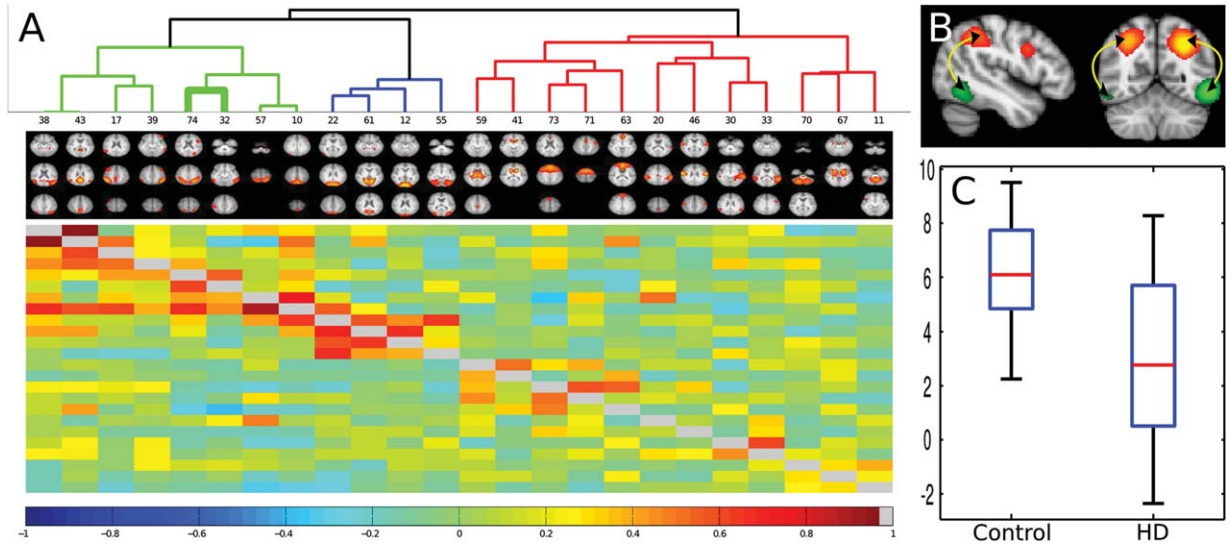

Figure 4.

Long-range functional connectivity in HD and controls. **A:** The dendrogram presents the heat map (correlation coefficients) between the time-series of all independent component analyses. Below the diagonal Fisher's *r* of the full correlations, and above the diagonal Fisher's *r* of the partial correlations are illustrated. The color bar shows the correlation coefficient. The thick lines between IC 74 and 32 indicate tighter coupling in controls as opposed to HD. **B:** Illustration of higher connectivity between ICA 74 (red-yellow, $5 < z < 12$) and ICA 32 (green, $5 < z < 10$). Voxel-coordinates in MNI-space: $x = 34$, $y = 68$. **C**: Box-plot of connection strengths. *Y*-axis: *z*-transformed *r* values of partial correlations.

strengths between ICA maps 32 and 74 (p=0.026, FWE corrected, indicated by the thick lines in Fig. 4), with a decrease in connectivity values in HD. Complementary to the analysis of the RSNs themselves, this approach demonstrated a reduction of inter-RSN connectivity in HD for a connection between parieto-occiptal RSNs that are part of the hierarchical cluster also comprising the DMN.

Impact of Motion Artifacts

Absolute displacement values did not differ significantly between groups (mean ± SD: Controls 0.40 ± 0.25 mm, HD 0.55 ± 0.30 mm; $t_{30.5} = -1.558$, $p = 0.130$). However, there was a marginally significant difference in micro-motion/relative displacement between groups with HD patients exhibiting more micro-motion (Controls: 0.12 ± 0.06 mm, HD 0.18 ± 0.11 mm; $t_{24.4} = -2.164$, $p = 0.041$). We did not detect a significant correlation between UHDRS motor scores and subject-wise averaged absolute displacement values (Spearman's rho $r_S = 0.21$, $p = 0.423$) or relative displacement values ($r_S = 0.09$, $p = 0.725$).

On average, relative displacement between volumes did not show a relevant correlation with ICA timecourses. The highest values were found for IC 37 and 81 ($r_S = 0.19$ and −0.20, respectively). Both ICAs were not part of our set of ICA maps of interest as described above and were compatible with brainstem motion (IC 37) and white matter signal artifacts (IC 81; data not shown).

DISCUSSION

This study provides evidence for abnormal functional connectivity networks in HD. After controlling for structural degeneration and age, we found widespread HD-related alterations of functional brain connectivity at rest using ICA of rs-fMRI data. First of all, compared with controls HD patients showed increased functional connectivity in a multitude of discrete subcortical and cortical networks, including the striatum, thalamus, prefrontal, premotor, and parietal cortices, along with core regions of the DMN such as the precuneus and anterior cingulate cortex. Second, correlations with parameters of clinical disease progression (i.e., UHDRS motor and TFC scores) again demonstrated an increase in local functional connectivity measures in mainly (pre)motor, sensorimotor, and parietal regions as well as in the middle cingulate cortex and precuneus. Increases in functional connectivity of fronto-striato-thalamo-cerebellar RSNs seemed to discriminate between HD patients and controls, while alterations in functional connectivity of fronto-parietal RSNs further modulated motor abilities and abilities of every-day living in patients. Third, whereas in HD short-range connectivity values were significantly higher than in controls, long-range connections between parieto-occipital RSNs were reduced at least between two RSNs, indicating a HD-related failure of functional coupling between RSNs. Overall, our data clearly demonstrate abnormal network connectivity in HD indicating that rs-fMRI may be a

promising, non-invasive and easily applicable clinical tool to measure early neuronal dysfunction beyond structural degeneration in HD.

Only few studies have investigated functional connectivity integrity in HD, which were mostly performed in premanifest HD mutation carriers and employed different analytical techniques complementing our findings. A task-based functional connectivity study in premanifest HD revealed lower attention-related connectivity within DMN subsystems (i.e., the anterior medial prefrontal, left inferior parietal cortex and posterior cingulate cortex), while the network connectivity between two DMN subsystems was greater in premanifest HD compared to controls [Wolf et al., 2012]. Since lower connectivity in the inferior parietal cortex was associated with shorter reaction times in the attention task, the authors suggested that specific DMN nodes might have to remain active to maintain cognitive performance in contrast to downregulation of these networks as observed in controls [Wolf et al., 2012]. In symptomatic HD, task-related functional connectivity (Simon task) between the anterior cingulate and lateral prefrontal cortex was reduced in patients indicating impaired coupling between functional networks, despite the fact that within these prefrontal regions HD patients showed increased BOLD activation during task performance compared to controls [Thiruvady et al., 2007]. In our analysis using ICA of fMRI data *at rest* we observed increased coactivation within neural networks along with a decrease in functional coupling between parieto-occipital RSNs. Unschuld et al. [2012] assessed seed-based resting-state connectivity in premanifest HD between the caudate and cortical seeds and found reduced BOLD synchrony between the caudate and premotor cortex [Unschuld et al., 2012]. In an MRI perfusion study of resting-state regional cerebral blood flow (rCBF) obtained with continuous arterial spin labeling, Wolf et al. [2011] reported less rCBF in premanifest HD than controls in the medial prefrontal cortex and increased rCBF in the left precuneus. Participants nearer to clinical onset additionally showed reduced rCBF in the left putamen as well as increased rCBF in the right hippocampus [Wolf et al., 2011]. Taken together and despite different methodological approaches, these studies indicate early functional connectivity changes in premanifest states, which seem to converge to a more general pattern of increased resting-state connectivity within network hubs and failure of functional coupling between these networks in the early manifest state. Enhanced functional activation in HD have been reported before in functional imaging studies, particularly in the symptomatic stage, which have been discussed as compensatory processes due to striatal or cortical degeneration [Georgiou-Karistianis, 2009; Paulsen, 2009]. Considering that we assessed coactivation patterns of BOLD-response at rest and controlled for structural degeneration, it is also possible that the increased RSN activity in HD might reflect a generalized spreading of activity due to reduced specialization of function in terms of a decrease in intra-network distinctiveness [Li et al., 2001; Rajah and D'Esposito, 2005]. This notion of a dedifferentiation process of function underlying enhancements in functional activity has been postulated for cognitive functioning in the aging brain [Li et al., 2001; Rajah and D'Esposito, 2005] and might also apply to changes in resting-state connectivity in neurodegenerative disease such as HD. In particular, we found alterations in HD-specific structures such as fronto-striato-thalamic networks, with an additional involvement of parts of the DMN. Against this backdrop of disturbed fronto-striato-thalamic and DMN connectivity, alterations of frontoparietal circuits seem to further modulate the clinical phenotype in terms of motor and TFC abilities. Core regions of the DMN, encompassing the medial prefrontal cortex, posterior cingulate cortex, precuneus, and lateral parietal cortices [Raichle et al., 2001; Raichle and Snyder, 2007], contributed rather little to TFC scores, with a p-value just short of formal significance ($p=0.056$). While there was considerable overlap in both correlation analyses with clinical scores (UHDRS motor and TFC) with respect to the RSNs involved, TFC seems to be associated with pathology of thalamus and caudate nucleus in addition to aforementioned frontoparietal RSNs. The absence of significant associations between resting-state connectivity and CAG repeat length or burden of disease pathology accords with findings in task-related functional connectivity analysis and resting-state rCBF measurements [Thiruvady et al., 2007; Wolf et al., 2011, 2012]. However, it might be argued that with exceeding a certain length threshold, a ceiling effect in terms of functional connectivity pathology could be reached. Analyses of subjects in the intermediate (27–35 repeats) or reduced penetrance range (36–39 repeats), none of which were present in our sample, might be better suited to reveal CAG-length dependent changes in functional connectivity.

Several previous fMRI studies highlighted an essential role of the DMN in neurodegenerative disorders such as Alzheimer's Disease [Greicius et al., 2004; Li et al., 2002] and Parkinson's disease [Tessitore et al., 2012]. Additionally, alterations in subcortical RSNs, which have received rather little attention, seem to be more pronounced in HD, particularly in the thalamus and striatum. Degeneration of the striatum starts several years prior to symptom manifestation and is the neuropathological hallmark in HD [Tabrizi et al., 2009; Vonsattel, 2008]. Thus, the brunt of the degenerative process involves the striatum, a key component of the basal ganglia, an interconnected set of subcortical nuclei involved in the regulation of action [Balleine et al., 2009]. Thalamic degeneration as well as dysfunctional thalamic metabolism have been shown to be an early feature in HD [Feigin et al., 2007; Kassubek et al., 2005]. In neurodegenerative disorders, increasing evidence suggest that pathology may begin within key vulnerable „hubs", central nodes interconnecting distinct, functionally specialized systems [Buckner et al., 2009]. These nexuses are upmost intriguing given their potential position in integration, and also because they may augment metabolic cascades relevant to

brain disease [Buckner et al., 2009]. It has also been argued that the diverse neurodegeneration syndromes target distinctive neuronal structures characterized by their connectivity properties that can be delineated by using task-free fMRI [Seeley et al., 2009]. The notion is that the neurodegenerative process spreads primarily to and between neurons that are interconnected perhaps according to their functional proximity to specific brain regions that act as critical hub-like „epicenters" [Zhou et al., 2012]. Our data seem compatible with that notion by showing that the striatum in HD is also one of the main vulnerable hubs on the level of functional connectivity, thus complementing neuropathological and structural data.

In terms of distinct functional brain connectivity between HD and controls, we found evidence for alterations of both short- and long-range connectivity in HD. This is reminiscent of the idea of "small-world" properties of brain networks derived by graph theory [Bullmore and Sporns, 2009], which also proposes that a short-range/long-range dichotomy should be functionally meaningful, and pathways might in turn show differential vulnerability to molecular lesions. It has been suggested that with respect to disintegrating brain networks, one such simple dichotomy may apply to short- versus long-range connections. Concerning our findings, it would seem that the "small-worldness" of brain networks increases in the course of HD, as shown descriptively by the reduction in long-range connectivity between two parieto-occipital RSNs on the one hand, and the increase in local connectivity measures in 11 out of 24 RSNs on the other hand. However, a graph theoretical approach to the data would be needed to confirm this notion. It is further not clear if the change in long-range connectivity is specific to the particular connection between parieto-occipital regions, as more subtle alterations might have been eluded due to the number of subjects examined. Crucially, this very pattern of reduced long-range connectivity as well as increased short-range connectivity has been shown to be an artefact introduced by residual motion [Power et al., 2012]. However, this seems to be a particular problem for seed-based analyses, as a recent work on motion artifacts in ICA-based rs-fMRI showed an increase in connectivity *beyond* the original seed ICA (and not locally inside the ICA), at least on a descriptive level [Satterthwaite et al., 2012]. We addressed this issue by examining the effect of motion on ICA timecourses in our study and did not find a significant effect of subject motion on rs-fMRI timecourses, although there was a slight increase in micro-motion in the HD cohort as measured by volume-by-volume relative displacements. Additionally, the amount of relative motion did not correlate with UHDRS motor scores in patients. Hence, these analyses do not indicate a critical impact of subject motion on our ICA-based rs-fMRI findings. Interestingly, the strongest correlation between volume-by-volume motion levels and ICA signal could be found in artifactual ICA maps, supporting the notion that ICA-based approaches are better suited to account for difficult-to-handle, though at least structured noise.

Another limitation of this study is the small cohort of premanifest HD participants, as it might have been interesting to directly compare different disease stages in terms of rs-fMRI connectivity, not at least to broaden the range of our correlation analysis with clinical and genetic parameters of disease progression. However, future longitudinal studies are needed to assess resting-state connectivity changes during disease progression and the prognostic value of the same than our cross-sectional design could address this issue sufficiently. Nevertheless, our data provide evidence for massive abnormal neuronal dysfunction at rest in HD patients that cannot be attributed to the presence of regional structural degeneration. Along with the increasing trend to examine healthy and pathological brain activity in terms of network connectivity [Bullmore and Sporns, 2009; Church et al., 2009; Seeley et al., 2009], we showed that this non-invasive, fast and feasible approach is well suitable as a potential clinical application in HD. Specifically, connectivity analysis using ICA is a preferable methodological tool targeting the entirety of spontaneous brain signal fluctuations in contrast to seed-voxel based methods which are usually restricted to pre-selected foci.

CONCLUSIONS

This study demonstrates that resting-state functional connectivity architecture is profoundly altered in HD. Complementing previous structural and functional studies, we found marked changes in resting state activity patterns in the prefrontal cortex and thalamus, accompanied by changes in caudate nucleus, cortical motor areas and parts of the DMN, even after controlling for age and atrophy in HD. Clinical TFC and motor scores were modulated by connectivity values of parietal maps, illustrating the crucial role of both parietal cortex and of caudate nucleus, the pivotal structure in HD. Furthermore, inter-component network analysis revealed a breakdown of long-range connectivity in HD compared to controls indicating impaired network interaction in HD. Motion parameters did not seem to exert a significant influence on ICA timecourses. Overall, RSN analyses are highly powerful and easily applicable clinical tools to assess neurobiological changes in HD and may provide valuable insights into disruptions of functional circuits in HD.

ACKNOWLEDGMENTS

The authors would like to thank all the HD participants and healthy controls for their enduring collaboration and interest in this research. They further thank their study nurse Daniela Probst for her excellent recruitment help.

REFERENCES

Balleine BW, Liljeholm M, Ostlund SB (2009): The integrative function of the basal ganglia in instrumental conditioning. Behav Brain Res 199:43–52.

Beckmann CF, Smith SM (2004): Probabilistic independent component analysis for functional magnetic resonance imaging. IEEE Trans Med Imaging 23:137–152.

Behrens TE, Johansen-Berg H, Woolrich MW, Smith SM, Wheeler-Kingshott CA, Boulby PA, Barker GJ, Sillery EL, Sheehan K, Ciccarelli O, et al. (2003): Non-invasive mapping of connections between human thalamus and cortex using diffusion imaging. Nat Neurosci 6:750–757.

Benjamini Y, Yekutieli D (2001): The control of the false disocovery rate in multiple testing under dependency. Annals Stat 29: 1165–1188.

Buckner RL, Sepulcre J, Talukdar T, Krienen FM, Liu H, Hedden T, Andrews-Hanna JR, Sperling RA, Johnson KA (2009): Cortical hubs revealed by intrinsic functional connectivity: Mapping, assessment of stability, and relation to Alzheimer's disease. J Neurosci 29:1860–1873.

Bullmore E, Sporns O (2009): Complex brain networks: Graph theoretical analysis of structural and functional systems. Nat Rev Neurosci 10:186–198.

Church JA, Fair DA, Dosenbach NU, Cohen AL, Miezin FM, Petersen SE, Schlaggar BL (2009): Control networks in paediatric Tourette syndrome show immature and anomalous patterns of functional connectivity. Brain 132:225–238.

Dogan I, Eickhoff SB, Schulz JB, Shah NJ, Laird AR, Fox PT, Reetz K (2012): Consistent neurodegeneration and its association with clinical progression in Huntington's disease: A coordinate-based meta-analysis Neurodegener Dis:DOI: 339528. Epub ahead of print.

Feigin A, Tang C, Ma Y, Mattis P, Zgaljardic D, Guttman M, Paulsen JS, Dhawan V, Eidelberg D (2007): Thalamic metabolism and symptom onset in preclinical Huntington's disease. Brain 130:2858–2867.

Filippini N, MacIntosh BJ, Hough MG, Goodwin GM, Frisoni GB, Smith SM, Matthews PM, Beckmann CF, Mackay CE (2009): Distinct patterns of brain activity in young carriers of the APOE-epsilon4 allele. Proc Natl Acad Sci USA 106:7209–7214.

Folstein MF, Folstein SE, McHugh PR (1975): "Mini-mental state". A practical method for grading the cognitive state of patients for the clinician. J Psychiatr Res 12:189–198.

Fox MD, Raichle ME (2007): Spontaneous fluctuations in brain activity observed with functional magnetic resonance imaging. Nat Rev Neurosci 8:700–711.

Fox MD, Greicius M (2010): Clinical applications of resting state functional connectivity. Front Syst Neurosci 4:19.

Georgiou-Karistianis N (2009): A peek inside the Huntington's brain: Will functional imaging take us one step closer in solving the puzzle? Exp Neurol 220:5–8.

Greicius M (2008): Resting-state functional connectivity in neuropsychiatric disorders. Curr Opin Neurol 21:424–430.

Greicius MD, Srivastava G, Reiss AL, Menon V (2004): Default-mode network activity distinguishes Alzheimer's disease from healthy aging: Evidence from functional MRI. Proc Natl Acad Sci USA 101:4637–4642.

Huntington Study Group (1996): Unified Huntington's Disease Rating Scale: Reliability and consistency. Mov Disord 11:136–142.

Kassubek J, Juengling FD, Ecker D, Landwehrmeyer GB (2005): Thalamic atrophy in Huntington's disease co-varies with cognitive performance: a morphometric MRI analysis. Cereb Cortex 15:846–853.

Li SC, Lindenberger U, Sikstrom S (2001): Aging cognition: From neuromodulation to representation. Trends Cogn Sci 5:479–486.

Li SJ, Li Z, Wu G, Zhang MJ, Franczak M, Antuono PG (2002): Alzheimer Disease: Evaluation of a functional MR imaging index as a marker. Radiology 225:253–259.

Nichols TE, Holmes AP (2002): Nonparametric permutation tests for functional neuroimaging: A primer with examples. Hum Brain Mapp 15:1–25.

Oakes TR, Fox AS, Johnstone T, Chung MK, Kalin N, Davidson RJ (2007): Integrating VBM into the General Linear Model with voxelwise anatomical covariates. Neuroimage 34:500–508.

Paulsen JS (2009): Functional imaging in Huntington's disease. Exp Neurol 216:272–277.

Penney JB, Jr., Vonsattel JP, MacDonald ME, Gusella JF, Myers RH (1997): CAG repeat number governs the development rate of pathology in Huntington's disease. Ann Neurol 41:689–692.

Power JD, Barnes KA, Snyder AZ, Schlaggar BL, Petersen SE (2012): Spurious but systematic correlations in functional connectivity MRI networks arise from subject motion. Neuroimage 59:2142–2154.

Raichle ME, MacLeod AM, Snyder AZ, Powers WJ, Gusnard DA, Shulman GL (2001): A default mode of brain function. Proc Natl Acad Sci USA 98:676–682.

Raichle ME, Snyder AZ (2007): A default mode of brain function: A brief history of an evolving idea. Neuroimage 37:1083–1090; discussion 1097–1099.

Rajah MN, D'Esposito M (2005): Region-specific changes in prefrontal function with age: A review of PET and fMRI studies on working and episodic memory. Brain 128:1964–1983.

Satterthwaite TD, Wolf DH, Loughead J, Ruparel K, Elliott MA, Hakonarson H, Gur RC, Gur RE (2012): Impact of in-scanner head motion on multiple measures of functional connectivity: Relevance for studies of neurodevelopment in youth. Neuroimage 60:623–632.

Seeley WW, Crawford RK, Zhou J, Miller BL, Greicius MD (2009): Neurodegenerative diseases target large-scale human brain networks. Neuron 62:42–52.

Shoulson I, Fahn S (1979): Huntington disease: Clinical care and evaluation. Neurology 29:1–3.

Smith SM, Fox PT, Miller KL, Glahn DC, Fox PM, Mackay CE, Filippini N, Watkins KE, Toro R, Laird AR, et al. (2009): Correspondence of the brain's functional architecture during activation and rest. Proc Natl Acad Sci USA 106:13040–13045.

Smith SM, Nichols TE (2009): Threshold-free cluster enhancement: Addressing problems of smoothing, threshold dependence and localisation in cluster inference. Neuroimage 44:83–98.

Tabrizi SJ, Langbehn DR, Leavitt BR, Roos RA, Durr A, Craufurd D, Kennard C, Hicks SL, Fox NC, Scahill RI, et al. (2009): Biological and clinical manifestations of Huntington's disease in the longitudinal TRACK-HD study: Cross-sectional analysis of baseline data. Lancet Neurol 8:791–801.

Tabrizi SJ, Scahill RI, Durr A, Roos RA, Leavitt BR, Jones R, Landwehrmeyer GB, Fox NC, Johnson H, Hicks SL, et al. (2011): Biological and clinical changes in premanifest and early stage Huntington's disease in the TRACK-HD study: The 12-month longitudinal analysis. Lancet Neurol 10:31–42.

Tabrizi SJ, Reilmann R, Roos RA, Durr A, Leavitt B, Owen G, Jones R, Johnson H, Craufurd D, Hicks SL, et al. (2012): Potential endpoints for clinical trials in premanifest and early Huntington's disease in the TRACK-HD study: Analysis of 24 month observational data. Lancet Neurol 11:42–53.

Tessitore A, Esposito F, Vitale C, Santangelo G, Amboni M, Russo A, Corbo D, Cirillo G, Barone P, Tedeschi G (2012): Default-

mode network connectivity in cognitively unimpaired patients with Parkinson disease. Neurology 79:2226–2232.

Thiruvady DR, Georgiou-Karistianis N, Egan GF, Ray S, Sritharan A, Farrow M, Churchyard A, Chua P, Bradshaw JL, Brawn TL, Cunnington R (2007): Functional connectivity of the prefrontal cortex in Huntington's disease. J Neurol Neurosurg Psychiatry 78:127–133.

Unschuld PG, Joel SE, Liu X, Shanahan M, Margolis RL, Biglan KM, Bassett SS, Schretlen DJ, Redgrave GW, van Zijl PC, et al. (2012): Impaired cortico-striatal functional connectivity in prodromal Huntington's Disease. Neurosci Lett 514:204–209.

Vonsattel JP (2008): Huntington disease models and human neuropathology: Similarities and differences. Acta Neuropathol 115:55–69.

Wolf RC, Gron G, Sambataro F, Vasic N, Wolf ND, Thomann PA, Saft C, Landwehrmeyer GB, Orth M (2011): Magnetic resonance perfusion imaging of resting-state cerebral blood flow in preclinical Huntington's disease. J Cereb Blood Flow Metab 31: 1908–1918.

Wolf RC, Sambataro F, Vasic N, Wolf ND, Thomann PA, Saft C, Landwehrmeyer GB, Orth M (2012): Default-mode network changes in preclinical Huntington's disease. Exp Neurol 237: 191–198.

Zhang D, Raichle ME (2010): Disease and the brain's dark energy. Nat Rev Neurol 6:15–28.

Zhou J, Gennatas ED, Kramer JH, Miller BL, Seeley WW (2012): Predicting regional neurodegeneration from the healthy brain functional connectome. Neuron 73:1216–1227.

Zuo XN, Kelly C, Adelstein JS, Klein DF, Castellanos FX, Milham MP (2010): Reliable intrinsic connectivity networks: Test-retest evaluation using ICA and dual regression approach. Neuroimage 49:2163–2177.